



OPEN

Re-recognizing micro locations of nanoscale zero-valent iron in biochar using C-TEM technique

Kun Yang^{1,2,3}✉, Jialu Xu^{1,2,3}, Ming Zhang⁴ & Daohui Lin^{1,2,3}

Biochar supported nanoscale zero-valent iron (NZVI/BC), prepared commonly by liquid reduction using sodium borohydride (NaBH_4), exhibits better reduction performance for contaminants than bare NZVI. The better reducing ability was attributed to attachment of nanoscale zero-valent iron (NZVI) on biochar (BC) surface or into the interior pores of BC particles due to observations by scanning electron microscopy (SEM) and plan transmission electron microscopy (P-TEM) techniques in previous studies. In this study, cross-sectional TEM (C-TEM) technique was employed firstly to explore location of NZVI in NZVI/BC. It was observed that NZVI is isolated from BC particles, but not located on the surface or in the interior pores of BC particles. This observation was also supported by negligible adsorption and precipitation of $\text{Fe}^{2+}/\text{Fe}^{3+}$ and iron hydroxides on BC surface or into interior pores of BC particles respectively. Precipitation of Fe^{2+} and Fe^{3+} , rather than adsorption, is responsible for the removal of Fe^{2+} and Fe^{3+} by BC. Moreover, precipitates of iron hydroxides cannot be reduced to NZVI by NaBH_4 . In addition to SEM or P-TEM, therefore, C-TEM is a potential technique to characterize the interior morphology of NZVI/BC for better understanding the improved reduction performance of contaminants by NZVI/BC than bare NZVI.

Nanoscale zero-valent iron (NZVI), as an environmental friendly material has been widely used in recent decades to reduce contaminants such as Cr(VI), As(V), nitrates, and chlorinated organics^{1–6}. Biochar (BC) supported NZVI (NZVI/BC), prepared commonly by liquid-phase reduction method using sodium borohydride (NaBH_4) as reducing agent, has better ability in reducing pollutants than NZVI^{7–9}. The oxidation and agglomeration of NZVI can be effectively suppressed by BC, therefore, NZVI's surface energy and reduction activity can be maintained^{5,10–12}. In previous studies^{13–16}, by scanning electron microscopy (SEM) and plan transmission electron microscopy (P-TEM) techniques, it was observed that NZVI particles were loaded on the surface or in the interior pores of BC particles, which is responsible for the improved reduction ability of NZVI^{17–19}. Several possible ways were suggested to interpret the loading of NZVI on BC surface or in BC interior pores (i) $\text{Fe}^{2+}/\text{Fe}^{3+}$ ions are adsorbed on surface or into interior pores of BC and then be reduced to NZVI by NaBH_4 ^{15,20–22}, (ii) $\text{Fe}^{2+}/\text{Fe}^{3+}$ ions are hydrolyzed into precipitates of iron hydroxide, and then deposited on surface or into interior pores of BC particles for reduction to NZVI by NaBH_4 ²³, (iii) $\text{Fe}^{2+}/\text{Fe}^{3+}$ ions are reduced to NZVI by NaBH_4 in solutions and then deposited on BC surface or into the interior pores of BC particles^{20,21}.

SEM and P-TEM are widely used electron microscopy techniques with high resolution and high magnification to visualize the morphology of NZVI/BC as well as the location of NZVI^{24–26}. However, by collecting secondary electrons reflected from sample surface, SEM technique can only visualize the sample top surface but not the interior structures^{27,28}. For P-TEM technique, the accumulated signals of the sample from top to bottom including the interior structures can be obtained by collecting electrons through the sample²⁹. However, the accumulated signals of P-TEM are difficult to explore the interior structure of samples clearly because the interior structure signals are actually covered by the electron signals of top and bottom surfaces, i.e., there is a problem of superimposition for P-TEM technique^{30,31}. Both of SEM and P-TEM technique cannot explore the interior structure signals of NZVI/BC particle clearly, i.e., the attachment of NZVI particles on the surface of BC or in the interior pores of BC particles is still not be observed directly. If the location of NZVI is not on surface or in interior pores of BC particles, the attachment of NZVI on/or in BC cannot be employed to interpret the better reduction performance of NZVI/BC than bare NZVI for contaminants. Therefore, it's needed to explore the location of NZVI in NZVI/BC for better understanding the improved reduction performance of NZVI/BC than bare NZVI.

¹Department of Environmental Science, Zhejiang University, Hangzhou 310058, China. ²Key Laboratory of Environmental Pollution and Ecological Health of Ministry of Education, Hangzhou 310058, China. ³Zhejiang Provincial Key Laboratory of Organic Pollution Process and Control, Hangzhou 310058, China. ⁴Department of Environmental Engineering, China Jiliang University, Hangzhou 310028, China. ✉email: kyang@zju.edu.cn

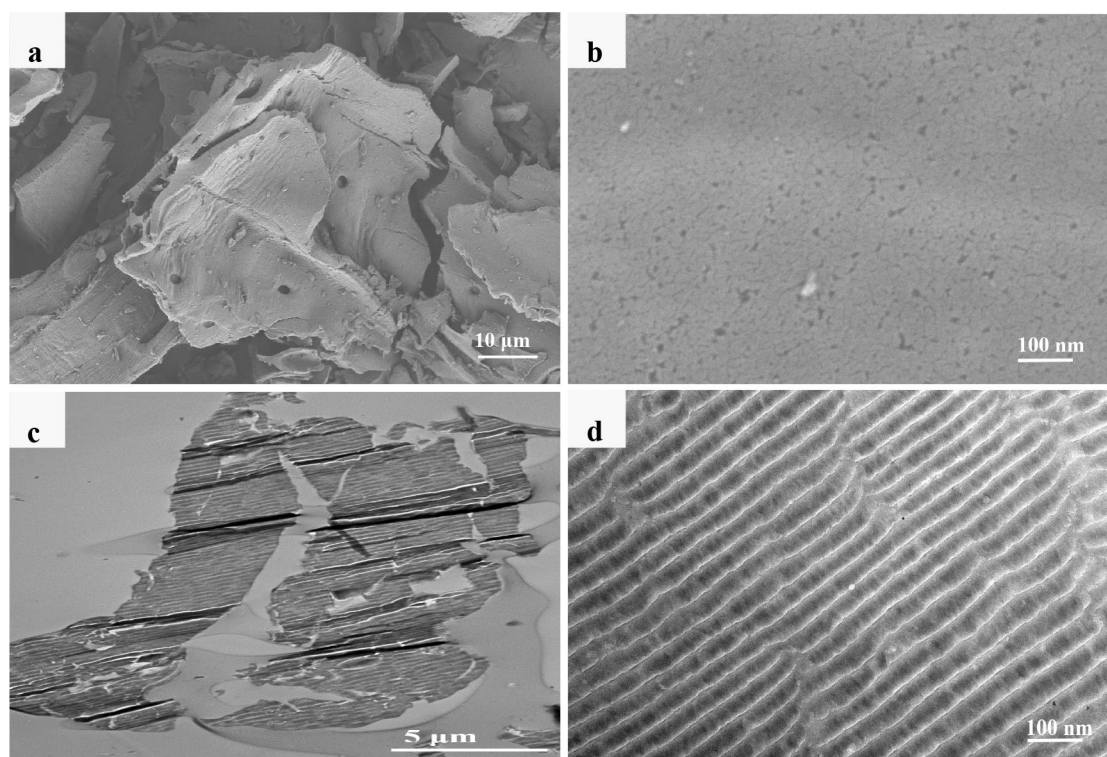


Figure 1. SEM images (a,b) and C-TEM images (c,d) of BC.

Cross-sectional TEM (C-TEM) technique, first reported in 1974³², is conducted through directly observing the inner ultra-thin slices (with thickness less than 100 nm) of samples using P-TEM technique. This technique can eliminate the problem of superimposition of P-TEM technique by avoiding the interfering of the sample surface signals, and thus, obtain the pure signals of interior structure of the sample^{33–35}. Therefore, C-TEM technique has been applied widely in characterizing of solid materials such as bulk heterojunction films^{36,37}, biochar³⁸, and activated carbons³⁹ in previous studies. In this study, therefore, C-TEM technique was firstly employed to directly identify the interior structures of NZVI/BC, especially the micro locations of NZVI in NZVI/BC particles. The comparison of the pH-dependent percent removal curves of metal cations under the presence of solid materials with the pH-dependent precipitation curves of metal cations without solid materials, a successful method established to identify whether the removal of metal cations with solid materials is adsorption or not in our previous studies^{40,41}, was employed here to explore whether the removal of Fe²⁺ or Fe³⁺ ions with BC is adsorption or not. If the two curves overlapped, the removal of Fe²⁺ or Fe³⁺ in the presence of BC should be attributed primarily to precipitation but not adsorption⁴⁰. If the removal of Fe²⁺ or Fe³⁺ with BC is by adsorption, the pH-dependent percent removal curve should be over the precipitation curve at some given pH⁴¹. Reduction experiments of Fe(OH)₂ and Fe(OH)₃ by NaBH₄ was also conducted here to explore whether the adsorbed Fe(OH)₂ or Fe(OH)₃ on BC can be reduced by NaBH₄. These experiments and the results could be helpful for exploring the underlying mechanisms to explain the better reduction performance of NZVI/BC than bare NZVI for contaminants.

Results and discussion

The surface morphology of BC particles observed by SEM technique is relatively smooth in lamellar structure (Fig. 1a), with abundant irregular pores (Fig. 1b). However, in C-TEM images (Fig. 1c,d), the slices of BC particles are in the sheet-like shape, showing abundant slit pores in uniform pore size. Bare NZVI particles in SEM (Fig. 2a) and C-TEM (Fig. 2b) images are roughly spherical and aggregated significantly to a chain-like structure, which should be attributed to the intrinsic magnetic attraction between the NZVI particles^{4,5,12,42,43}. There are a lot of chain-like clusters and roughly spherical particles dispersed on BC surface in SEM images of NZVI/BC (Fig. 3a,b). These chain-like clusters and roughly spherical particles on the surface of NZVI/BC are NZVI particles, as was also observed by the SEM images of bare NZVI particles (Fig. 2a) and NZVI/BC in previous studies^{11,16,18,42}. EDX spectrum of NZVI/BC shows that the main elemental composition of NZVI/BC is C, Fe and O (Fig. 3c). The homogeneous distribution of C and Fe was also verified in SEM elemental mapping of NZVI/BC (Figure S1). NZVI particles formed in NZVI/BC are identified by the characteristic peak at 44.7° (Fig. 3d) of XRD pattern of NZVI/BC. NZVI particles formed and dispersed on the surface of NZVI/BC were also observed in P-TEM images of NZVI/BC in previous studies^{19,22}. However, in C-TEM images of NZVI/BC (Fig. 4a and Figure S1), NZVI particles are existed isolated from BC particles rather than attached on the surface of BC particles. The distinguished observations in C-TEM images of NZVI/BC from that in SEM and P-TEM images of NZVI/BC, could be attributed to the top surface view of SEM technique^{27,29} and the superimposition problem of

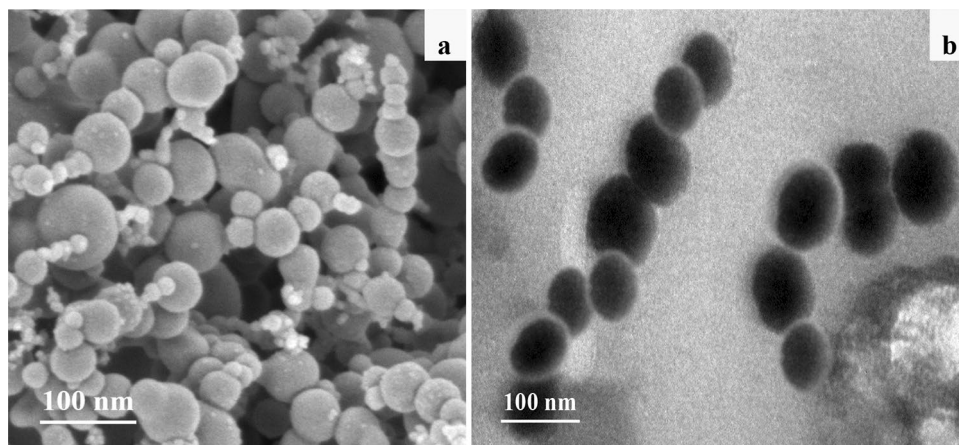


Figure 2. SEM image (a) and C-TEM image (b) of NZVI.

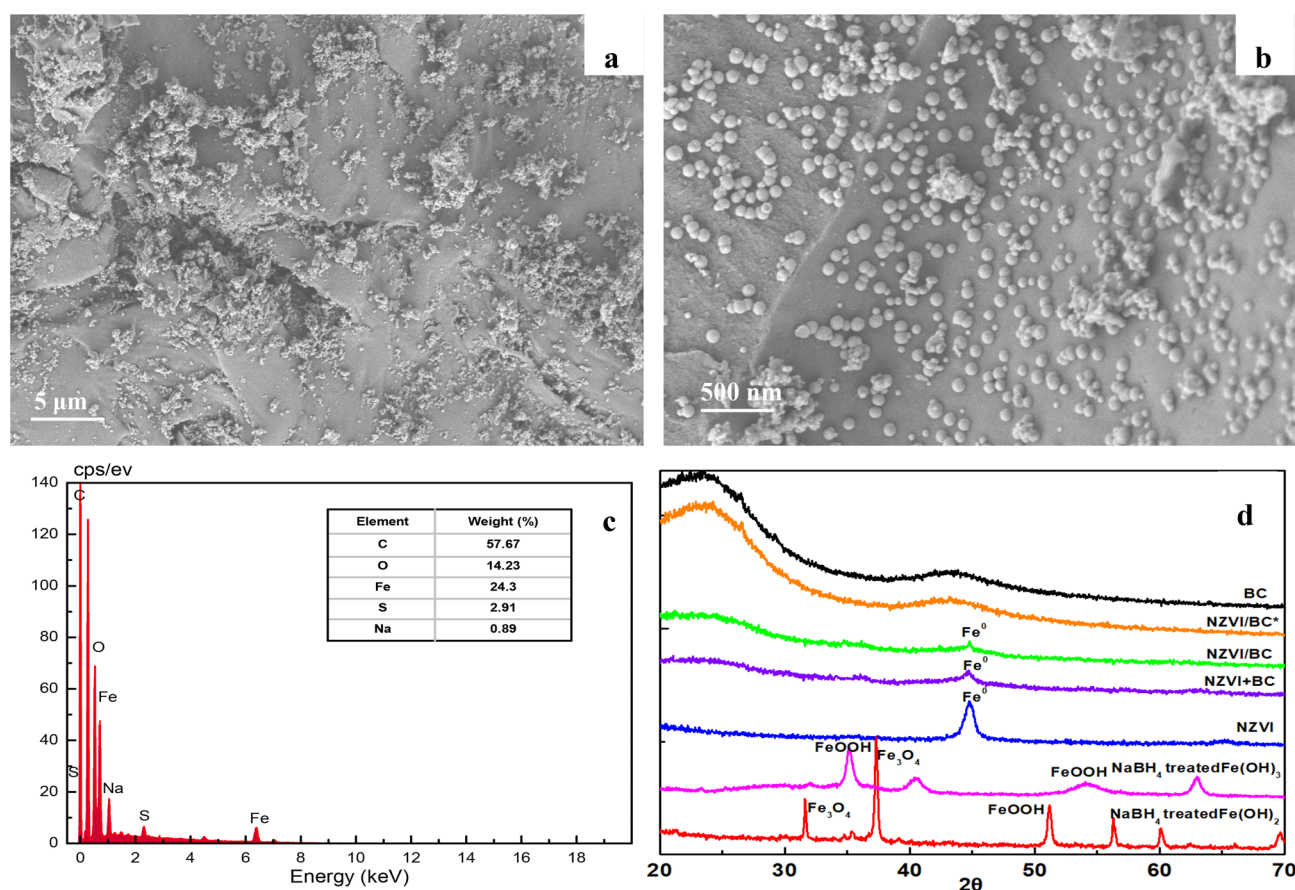


Figure 3. SEM images (a,b) and EDX (c) spectrum of NZVI/BC, as well as XRD patterns (d) of BC, NZVI/BC, NZVI/BC*, NZVI+BC, NZVI, NaBH_4 treated $\text{Fe}(\text{OH})_2$ and NaBH_4 treated $\text{Fe}(\text{OH})_3$.

P-TEM technique^{30,31}. Thus, both of SEM and P-TEM techniques cannot explore the interior structure signals of NZVI/BC particles. Moreover, NZVI particles are not observed in interior slit pores of BC particles (Fig. 4b and Figure S1), i.e., NZVI particles cannot be embedded into the interior pores of BC particles. As reported in the previous literatures^{11,44,45}, the average particle size of NZVI on NZVI/BC is about 30–100 nm. In this study, the particle size of NZVI in NZVI/BC is in the range of 40–180 nm (Fig. 3b). However, BC is basically composed of micropores and mesopores with average diameter less than 10 nm^{13,38,46}. The N_2 adsorption–desorption isotherm and pore size distribution of BC in this study are shown in Figure S3. The specific surface and average pore size of BC are 579.15 m^2/g and 2.486 nm, respectively. Therefore, NZVI particles cannot enter into interior pores of BC particles, showing the clean and slit pores without any iron particles in C-TEM images of NZVI/BC (Fig. 4). In addition, the surface morphology of NZVI/BC in SEM images (Fig. 3a,b) and inner cross section structure

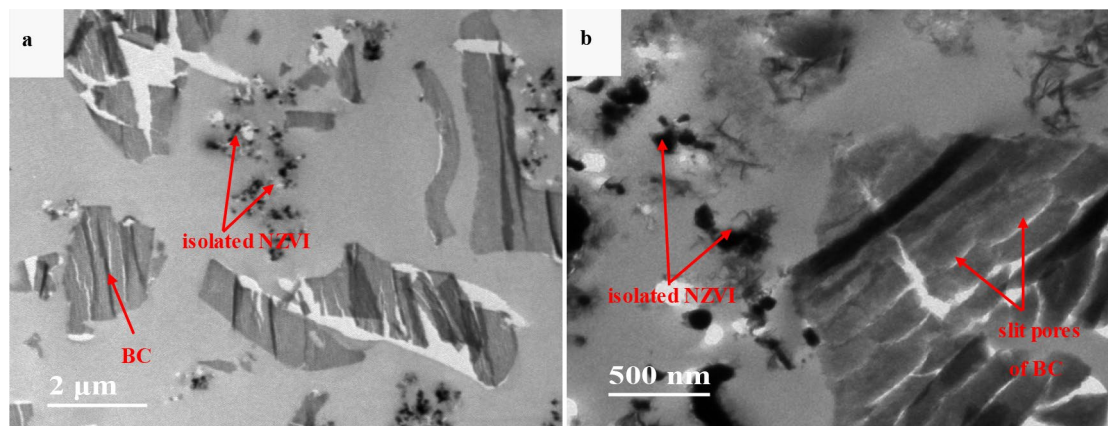


Figure 4. C-TEM images (a,b) of NZVI/BC.

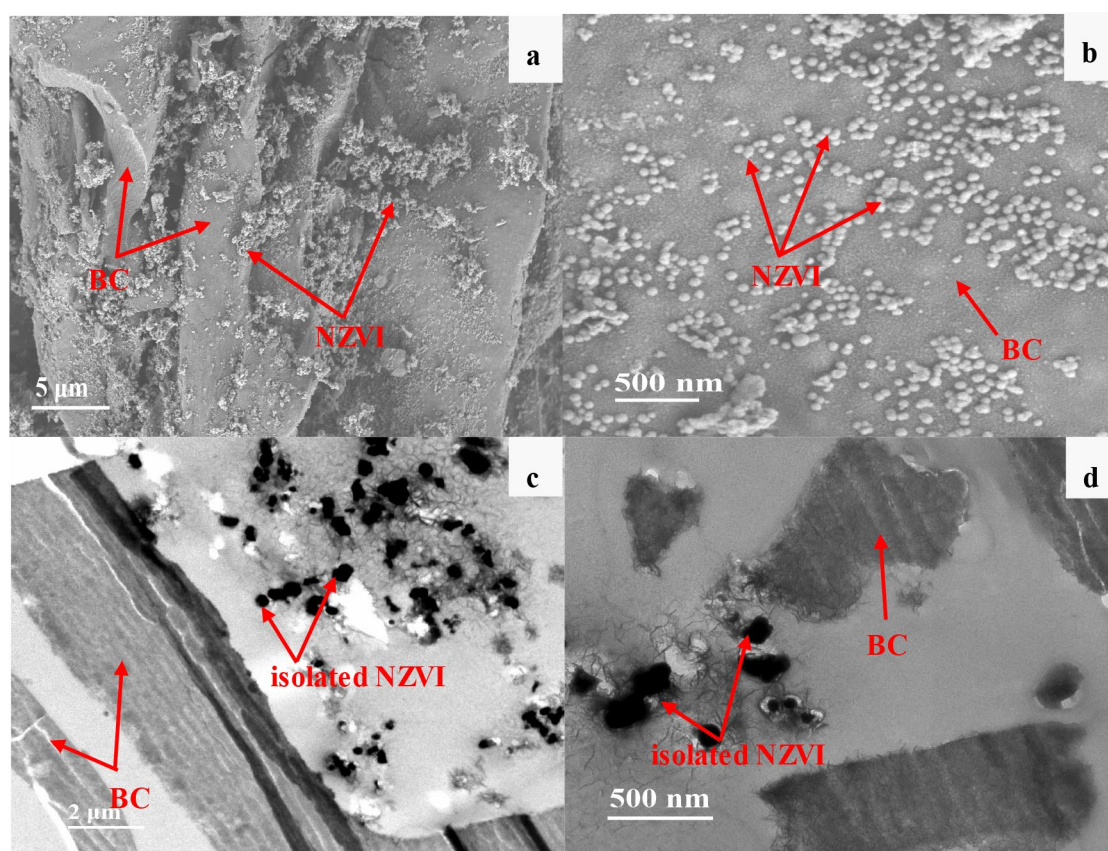


Figure 5. SEM (a,b) and C-TEM images (c,d) of NZVI+BC.

of NZVI/BC in C-TEM images (Fig. 4) as well as the XRD pattern (Fig. 3d) of NZVI/BC are similar to that of NZVI+BC (Figs. 3d and 5), the sample mixed from NZVI and BC directly. Therefore, NZVI/BC is similar to NZVI+BC, without attachment of NZVI on BC surface or into BC interior pores, i.e., the better reduction ability of NZVI/BC for contaminants than NZVI cannot be interpreted by the attachment of NZVI on BC surface or into BC interior pores.

Adsorption of Fe^{2+} or Fe^{3+} ions on BC and then reduction of adsorbed Fe^{2+} or Fe^{3+} ions by NaBH_4 was proposed as a possible way to load NZVI on BC surface or in BC interior pores^{15,20–22}. However, we observed that the removal curves of Fe^{3+} in the presence of BC under various pH overlapped with the precipitation curve of Fe^{3+} without BC (Fig. 6a,b). Moreover, removal curves of Fe^{3+} were independent of the dosage of BC (20 and 200 mg) in Fig. 6a or initial concentration of Fe^{3+} (50 and 150 mg/L) in Fig. 6b. Therefore, the removal of Fe^{3+} ions in the presence of BC should be attributed primarily to precipitation by formation of $\text{Fe}(\text{OH})_3$, rather than adsorption on BC⁴⁰. Although the removal curve of Fe^{2+} didn't overlapped with the precipitation curve of Fe^{2+}

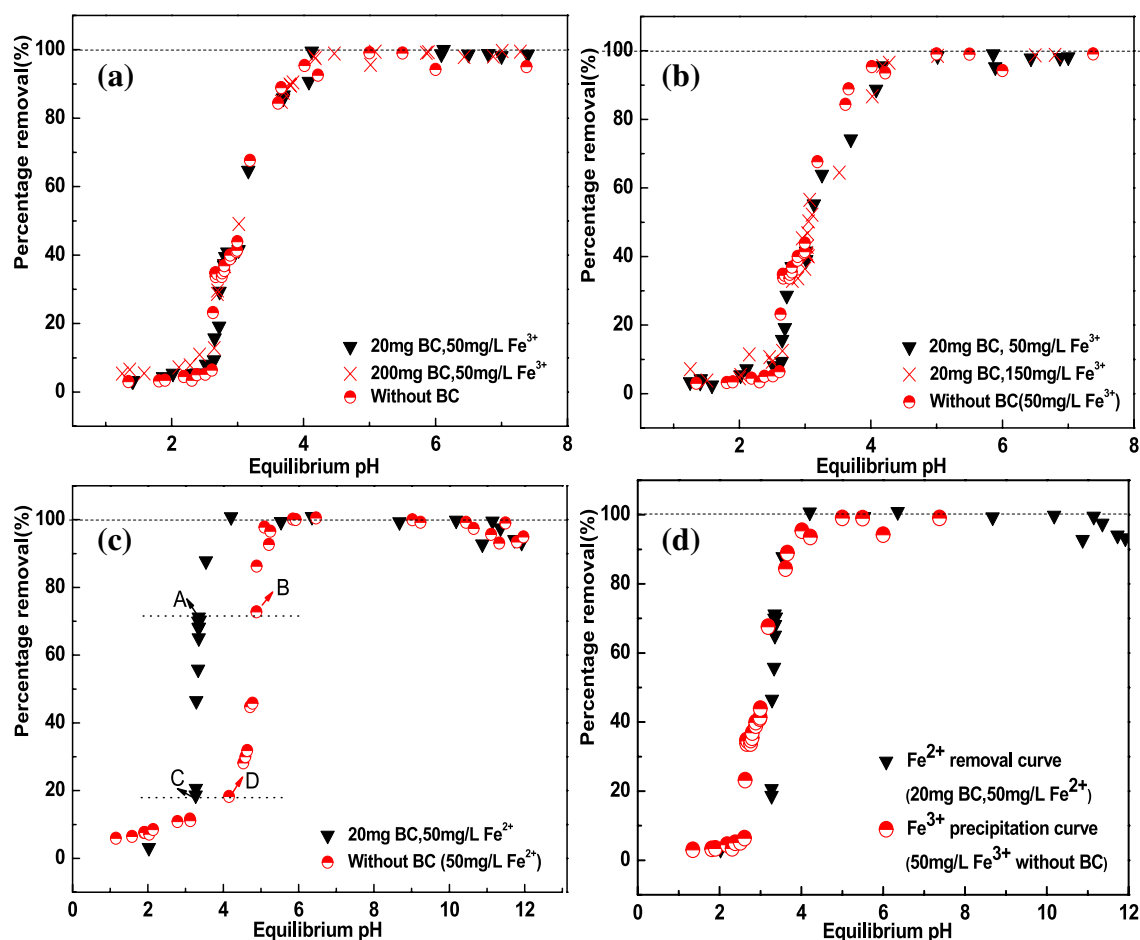


Figure 6. pH-dependent percent removal curves of Fe^{3+} or Fe^{2+} with or without BC. The used BC dose for Fe^{3+} are 0, 20, 200 mg in 20 mL solution (a), while that for Fe^{2+} are 0 and 20 mg (c). The employed concentration of Fe^{3+} are 50 and 150 mg/L (b), while that of Fe^{2+} is 50 mg/L (c,d).

without BC (Fig. 6c), it overlapped with the precipitation curve of Fe^{3+} without BC (Fig. 6d), implying that the oxidation of Fe^{2+} to Fe^{3+} and then the precipitation of Fe^{3+} may be responsible for the removal of Fe^{2+} with BC. In order to check this hypothesis, four different points (A, B, C, D) were chosen to determine the mass of Fe^{2+} and Fe^{3+} in supernatants and solids, respectively (Fig. 6c). Species distribution of Fe^{2+} and Fe^{3+} in supernatant and solids are listed in Table S1. Oxidation of Fe^{2+} to Fe^{3+} with or without BC were observed (Table S1). In the presence of BC and higher pH, more Fe^{2+} were oxidized to Fe^{3+} (Table S1). Therefore, the oxidation of Fe^{2+} to Fe^{3+} occurred in batch experiment for Fe^{2+} by BC. Characteristic peak of NZVI was not observed in XRD diffraction pattern of NZVI/BC*, a sample prepared by removing excessive free Fe^{2+} in Fe^{2+} /BC system before adding NaBH_4 (Fig. 3d), indicating almost no Fe^{2+} or Fe^{3+} adsorbed on BC. Moreover, the C-TEM diagrams of NZVI/BC* were similar to that of BC (Figures S4), indicating that no black NZVI particles observed in NZVI/BC, i.e., no Fe^{2+} or Fe^{3+} adsorption on BC observed. Therefore, Fe^{2+} and Fe^{3+} cannot be fixed on BC surface or in interior pores through adsorption to form NZVI on BC by reduction using NaBH_4 .

Forming of $\text{Fe}(\text{OH})_2$ or $\text{Fe}(\text{OH})_3$ precipitates, deposited on BC and then reduced to NZVI by NaBH_4 was proposed as another possible way to load NZVI on BC surface or in BC interior pores^{21,23}. However, depositing of $\text{Fe}(\text{OH})_2$ or $\text{Fe}(\text{OH})_3$ precipitates on the surface or in the interior pores of BC particles were not observed in C-TEM images of NZVI/BC* (Figure S4), showing that the surface and pores of NZVI/BC* are clean and similar to that of BC (Figure S4). Moreover, NZVI can be obtained by reducing iron salt with NaBH_4 rather than hydroxide^{4,47}, i.e., $\text{Fe}(\text{OH})_2$ or $\text{Fe}(\text{OH})_3$ cannot be reduced to NZVI by NaBH_4 . For example, the suspensions of dark green $\text{Fe}(\text{OH})_2$ precipitates and reddish brown $\text{Fe}(\text{OH})_3$ precipitates (Fig. 7a), prepared from Fe^{2+} and Fe^{3+} respectively via chemical precipitation, are not changed in color after dropping NaBH_4 (Fig. 7b) under nitrogen atmosphere, i.e., No black ZVI particles formed after reduction treatment of $\text{Fe}(\text{OH})_2$ and $\text{Fe}(\text{OH})_3$ precipitates with NaBH_4 . The characteristic peak of NZVI was not observed in XRD diffraction patterns of the dried solid samples collected from NaBH_4 treated $\text{Fe}(\text{OH})_2$ and NaBH_4 treated $\text{Fe}(\text{OH})_3$ (Fig. 3d), indicating NZVI cannot be obtained from $\text{Fe}(\text{OH})_2$ and $\text{Fe}(\text{OH})_3$ precipitates by reduction using NaBH_4 . Therefore, NZVI cannot be loaded on BC via depositing of $\text{Fe}(\text{OH})_2/\text{Fe}(\text{OH})_3$ precipitates on surface or into interior pores of BC particles as well as reduction of $\text{Fe}(\text{OH})_2/\text{Fe}(\text{OH})_3$ precipitates to NZVI by NaBH_4 .

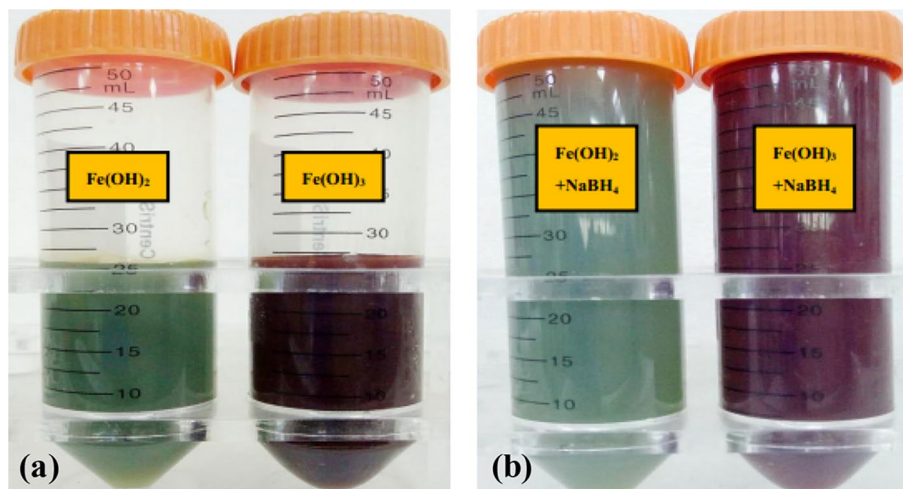


Figure 7. Pictures of suspensions of $\text{Fe}(\text{OH})_2$ and $\text{Fe}(\text{OH})_3$ precipitates before (a) and after treated with NaBH_4 solution (b).

Except for loading of NZVI on the surface or into the interior pores of BC, smaller size of NZVI in NZVI/BC was proposed to interpret the better reduction performance of contaminants by NZVI/BC than bare NZVI^{5,22,42}. Smaller-sized NZVI is more reactive, which can be attributed to its higher surface area-to-volume ratio and stronger quantum effects^{4,6,11}. In this study, bare NZVI particles are aggregated into micron-size particles (Fig. 2), which is consistent with the previous reports^{6,42,48}. However, the particle size of NZVI in NZVI/BC is in the range of 40–180 nm (Figs. 3b and 4), much smaller than that of bare NZVI (Fig. 2), implying that the agglomeration of NZVI particles is effectively alleviated by BC^{10,22}. The alleviation of NZVI agglomeration was also observed in sample NZVI + BC, showing that the particle size of NZVI in NZVI + BC is in the range of 50–220 nm (Fig. 5). Therefore, the smaller size of NZVI in NZVI/BC than that of bare NZVI could be possibly responsible for the better reduction performance of contaminants by NZVI/BC than bare NZVI^{10–12}. In previous studies^{10,13,42}, the smaller size of NZVI in NZVI/BC was attributed to the attachment of NZVI on BC surface or into the interior pores of BC particles that inhibit the aggregation of NZVI. However, in this study, the observed smaller size of NZVI in NZVI/BC should be attributed to the mixing of NZVI with BC that inhibit the aggregation of NZVI, but not the attachment of NZVI on/in BC particles.

Conclusion and outlook

Employing C-TEM technique for liquid reduction method prepared NZVI/BC, it was observed in this study that NZVI particles are existed isolated from BC particles in NZVI/BC, rather than attached on surface or in interior pores of BC particles that was observed in previous study by SEM and P-TEM techniques. This observation was also supported by the negligible adsorption of $\text{Fe}^{2+}/\text{Fe}^{3+}$ and the negligible attachment of $\text{Fe}(\text{OH})_2/\text{Fe}(\text{OH})_3$ precipitates on BC surface or interior pore structure of BC particles, as well as the negligible reduction of $\text{Fe}(\text{OH})_2/\text{Fe}(\text{OH})_3$ to NZVI by NaBH_4 . Therefore, both of the widely used SEM and P-TEM techniques have difficulty in observing the inner structure of NZVI/BC. In addition to SEM and P-TEM, C-TEM is a useful technique to characterize the interior morphology of NZVI/BC and other porous materials supported NZVI for better exploring their underlying improved reduction performance of contaminants. Besides, C-TEM can also be employed to characterize the interior morphology and configuration of other composite materials. The better reduction performance of NZVI/BC than bare NZVI could be attributed to the smaller size of NZVI particles in NZVI/BC, due to mixing NZVI with BC particles, which inhibit the aggregation of NZVI, but could not be explained by the attachment of NZVI particles on surface or into interior pores of BC particles in NZVI/BC.

Materials and methods

Chemicals. Ferrous sulfate heptahydrate ($\text{FeSO}_4 \cdot 7\text{H}_2\text{O}$, 97%), sodium borohydride (NaBH_4 , 98%), and hydroxylamine hydrochloride ($\text{NH}_2\text{OH} \cdot \text{HCl}$, 99%) were supplied by Sinopharm Group Chemical Reagent, China. Ferric chloride hexahydrate ($\text{FeCl}_3 \cdot 6\text{H}_2\text{O}$, 99%) was obtained from Aladdin Reagent Corporation.

Preparation of BC and NZVI materials. BC was prepared from wood chips (Ningbo, Zhejiang, China) by oxygen-limited pyrolysis method⁴⁹. Briefly, dried wood chips, grounded to pass through a 0.15 mm sieve, were packed in crucibles, covered with lids, and then, placed in a muffle furnace, pyrolyzed at 700 °C for 6 h. The prepared BC was washed with 1 mol/L HCl ($m/v=0.1$ g/mL) by stirring for 24 h to remove impurities and then rinsed using deionized (DI) water to neutral pH. The obtained BC sample was dried overnight at 80 °C in an oven for usage.

Bare NZVI was synthesized using the liquid-phase reduction method^{11,12,50}. Briefly, under nitrogen atmosphere, 100 mL NaBH_4 solution (1.2 mol/L) was dropped (1–2 drops/s) into 100 mL FeSO_4 solution (0.44 mol/L) with stirring. The black NZVI particles were separated by centrifugation for 5 min at 3000 rpm. Then, NZVI

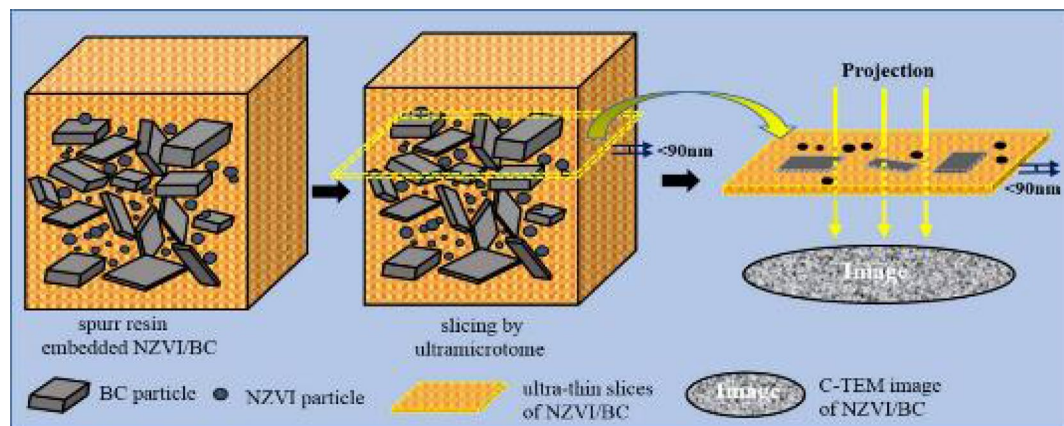


Figure 8. Schematic of ultra-thin slice of NZVI/BC preparation.

particles were washed with deoxygenated DI water, followed by ethanol, and finally dried in a vacuum oven at $60\text{ }^{\circ}\text{C}$ for 12 h.

NZVI/BC was prepared according to the procedures reported in the previous literature⁵¹. Under nitrogen atmosphere, 100 mL of 0.44 mol/L FeSO_4 solution was mixed with 5.0 g BC for 3 h. Then, 100 mL of 1.2 mol/L NaBH_4 was added dropwise into the mixture. After reaction, NZVI/BC was collected by centrifugation at 3000 rpm for 5 min, washed with deoxygenated DI water and ethanol, and dried in a vacuum oven ($60\text{ }^{\circ}\text{C}$, 12 h).

NZVI/BC* was prepared as follows. 100 mL of 0.44 mol/L FeSO_4 solution was mixed with 5.0 g BC under nitrogen atmosphere for 24 h. Then the solid was collected by centrifugation at 3000 rpm for 5 min and followed by washing with deoxygenated DI water for three times to remove excess free Fe^{2+} that not adsorbed on BC. Under nitrogen atmosphere, 100 mL of 1.2 mol/L NaBH_4 was added dropwise into the suspension of BC which was pretreated with FeSO_4 solutions. Then, by centrifugation at 3000 rpm for 5 min, washed with deoxygenated DI water and ethanol, and dried in a vacuum oven at $60\text{ }^{\circ}\text{C}$ for 12 h, nNZVI/BC* was collected.

NZVI + BC was prepared directly by mixing BC and NZVI particles. Briefly, 1.0 g BC and 0.5 g NZVI were mixed in 30 mL ethanol in a beaker and dispersed by ultrasonic cell breaker (SCIENTZ-II D) for 10 min ($20\text{ }^{\circ}\text{C}$, 570 W). Then, the mixed NZVI + BC sample was separated by centrifugation at 3000 rpm for 5 min and dried in a vacuum oven ($60\text{ }^{\circ}\text{C}$, 12 h).

Characterization of BC and NZVI materials. The inner structure information of BC and NZVI materials was observed by C-TEM technique directly^{38,39}. These samples were firstly embedded into embedding agent, i.e., spurr resin, which is a mixture of 10 g vinyl cyclohexene dioxide (ERL 4221), 8 g diglycidyl ether of polypropylene glycol (DER 736), 25 g nonenyl succinic anhydride (NSA) and 0.3 g 2-dimethylaminoethanol (DMAE), purchased from SPI-Chem Supplies. Then, spurr resin embedded samples were heated at $70\text{ }^{\circ}\text{C}$ for 12 h, and cut into ultra-thin slices with thickness less than 90 nm by ultramicrotome (Leica, EMUC7, Germany) equipped with diamond knife (Fig. 8). The slices were finally collected on copper mesh grids for observation of TEM at 200 kV (JEM1200, JEOL, Japan).

X-ray diffraction patterns of samples were obtained by an X-ray diffractometer (XRD, Philips, Netherlands) equipped with a $\text{CuK}\alpha$ radiation source and scanned at a speed of 2° per min. Surface morphologies of samples were examined by using a field emission SEM (FE-SEM) (SIRON, FEI, Netherlands) equipped with an energy dispersive spectroscopy (Oxford Inca EDS) at a voltage of 25.0 kV.

Batch experiments for Fe^{2+} and Fe^{3+} by BC. Fe^{2+} and Fe^{3+} solution was prepared from $\text{FeSO}_4 \cdot 7\text{H}_2\text{O}$ and $\text{FeCl}_3 \cdot 6\text{H}_2\text{O}$ respectively. Batch experiment of Fe^{2+} and Fe^{3+} was conducted in 22 mL screw cap vials with a total solution volume of 20 mL sealed with Teflon-coated septa under ambient temperature ($25\text{ }^{\circ}\text{C}$). Briefly, 20 mg or 200 mg BC was added into vials having 18 mL background solution with various pH value, prepared from DI water with 0.01 mol/L HCl and NaOH. Then, 2 mL Fe^{2+} or Fe^{3+} solution (500 mg/L or 1500 mg/L), was added into the vials to give the initial Fe^{2+} or Fe^{3+} concentration of 50 mg/L or 150 mg/L, respectively. The vials were capped and transferred to a horizontal shaker (DHZ-D) at 150 rpm for 48 h. After centrifugation at 3000 rpm for 5 min, supernatant was taken from vials, and filtered with a $0.22\text{ }\mu\text{m}$ needle filter to remove the solid. The pH value of supernatant was measured using a glass pH electrode (Mettler Toledo). The concentration of Fe^{2+} iron in supernatant was determined by UV-spectrophotometer (UV-2450, Shimadzu, Japan) with 1,10-phenanthroline spectrophotometric method at a maximum wavelength of 510 nm ⁵². For measurement of Fe^{3+} , Fe^{3+} in supernatant was reduced to Fe^{2+} firstly by $\text{NH}_2\text{OH} \cdot \text{HCl}$ ⁵³, and then, determined by UV-spectrophotometer with 1,10-phenanthroline spectrophotometric method⁵².

The removal efficiency of Fe^{2+} or Fe^{3+} was calculated by Eq. (1):

$$\text{R}\% = (C_0 - C_e) / C_0 * 100\% \quad (1)$$

where C_0 (mg/L) is the initial concentration of Fe^{2+} or Fe^{3+} in solution, C_e (mg/L) is the equilibrium concentration of Fe^{2+} or Fe^{3+} in solution.

Precipitation experiments of Fe²⁺ and Fe³⁺ in aqueous phase. Precipitation of Fe²⁺ and Fe³⁺ was also conducted in 22 mL screw cap vials. 18 mL background water at various pH, prepared from DI water with 0.01 mol/L HCl and NaOH, and 2 mL Fe²⁺ or Fe³⁺ solution (500 mg/L) were mixed in the vials, i.e., the initial Fe²⁺ or Fe³⁺ concentration in vials was 50 mg/L. The vials were capped and transferred to a horizontal shaker (DHZ-D) at 150 rpm for 48 h under ambient temperature (25 °C). After centrifugation at 3000 rpm for 5 min, pH value and equilibrium concentration of Fe²⁺ or Fe³⁺ in supernatant were measured with glass pH electrode (Mettler Toledo) and UV-spectrophotometer (UV-2450, Shimadzu, Japan), respectively^{52,53}.

Reduction of Fe(OH)₂ and Fe(OH)₃ by NaBH₄. For reduction experiments of Fe(OH)₂ or Fe(OH)₃ precipitates by NaBH₄, 10 mL 0.25 M Fe²⁺ or Fe³⁺ solution and 10 mL 1.0 M NaOH solution were mixed and then centrifuged at 3000 rpm for 5 min to collect Fe(OH)₂ or Fe(OH)₃ precipitates. The collected Fe(OH)₂ or Fe(OH)₃ precipitate was washed with deoxidizing DI water for three times to remove excessive Fe²⁺ or Fe³⁺ ions. Before reduction by NaBH₄, another 20 mL deoxidizing DI water was added to redispense Fe(OH)₂ or Fe(OH)₃ precipitates. Then, 20 mL 1.0 M NaBH₄ was added dropwise under nitrogen atmosphere to reduce the precipitates. After reduction reaction, solid product was collected by centrifugation at 3000 rpm for 5 min, washed with deoxidizing DI water and ethanol, and finally dried in a vacuum oven at 60 °C for 12 h.

Received: 22 December 2020; Accepted: 16 February 2021

Published online: 03 March 2021

References

- Liu, S. C. *et al.* Study on influencing factors and mechanism of removal of Cr(VI) from soil suspended liquid by bentonite-supported nanoscale zero-valent iron. *Sci. Rep.* **10**, 8831 (2020).
- Ahmad, M. *et al.* Turning date palm waste into carbon nanodots and nano zerovalent iron composites for excellent removal of methylthionium chloride from water. *Sci. Rep.* **10**, 16125 (2020).
- Gil-Díaz, M., Álvarez, M. A., Alonso, J. & Lobo, M. C. Effectiveness of nanoscale zero-valent iron for the immobilization of Cu and/or Ni in water and soil samples. *Sci. Rep.* **10**, 15927 (2020).
- Wang, C. B. & Zhang, W. X. Synthesizing nanoscale iron particles for rapid and complete dechlorination of TCE and PCBs. *Environ. Sci. Technol.* **31**, 2154–2156 (1997).
- Zhao, X. *et al.* An overview of preparation and applications of stabilized zero-valent iron nanoparticles for soil and groundwater remediation. *Water Res.* **100**, 245–266 (2016).
- Zou, Y. *et al.* Environmental remediation and application of nanoscale zero-valent iron and its composites for the removal of heavy metal ions: A review. *Environ. Sci. Technol.* **50**, 7290–7304 (2016).
- Mackenzie, K., Bleyl, S., Kopinke, F. D., Doose, H. & Bruns, J. Carbo-Iron as improvement of the nanoiron technology: From laboratory design to the field test. *Sci. Total Environ.* **563**, 641–648 (2016).
- Diao, Z. H. *et al.* Insights into the simultaneous removal of Cr⁶⁺ and Pb²⁺ by a novel sewage sludge-derived biochar immobilized nanoscale zero valent iron: Coexistence effect and mechanism. *Sci. Total Environ.* **642**, 505–515 (2018).
- Qian, L. B. *et al.* Field demonstration of enhanced removal of chlorinated solvents in groundwater using biochar-supported nanoscale zero-valent iron. *Sci. Total Environ.* **698**, 134215 (2020).
- Dong, H. R. *et al.* Stabilization of nanoscale zero-valent iron (nZVI) with modified biochar for Cr(VI) removal from aqueous solution. *J. Hazard. Mater.* **332**, 79–86 (2017).
- Liu, C. M., Diao, Z. H., Huo, W. Y., Kong, L. J. & Du, J. J. Simultaneous removal of Cu²⁺ and bisphenol A by a novel biochar-supported zero valent iron from aqueous solution: Synthesis, reactivity and mechanism. *Environ. Pollut.* **239**, 698–705 (2018).
- Xu, J. *et al.* Iron and sulfur precursors affect crystalline structure, speciation, and reactivity of sulfidized nanoscale zerovalent iron. *Environ. Sci. Technol.* **54**, 13294–13303 (2020).
- Dong, H. R. *et al.* Removal of trichloroethylene by biochar supported nanoscale zero-valent iron in aqueous solution. *Sep. Purif. Technol.* **188**, 188–196 (2017).
- Liati, A. *et al.* Electron microscopic study of soot particulate matter emissions from aircraft turbine engines. *Environ. Sci. Technol.* **48**, 10975–10983 (2014).
- Zhu, S. *et al.* Magnetic nanoscale zerovalent iron assisted biochar: Interfacial chemical behaviors and heavy metals remediation performance. *ACS Sustain. Chem. Eng.* **5**, 9673–9682 (2017).
- Wei, A. L. *et al.* Enhanced nitrate removal and high selectivity towards dinitrogen for groundwater remediation using biochar-supported nano zero-valent iron. *Chem. Eng. J.* **353**, 595–605 (2018).
- Liu, W. J., Jiang, H. & Yu, H. Q. Development of biochar-based functional materials: Toward a sustainable platform carbon material. *Chem. Rev.* **115**, 12251–12285 (2015).
- Ahmed, M. B. *et al.* Nano-Fe-0 immobilized onto functionalized biochar gaining excellent stability during sorption and reduction of chloramphenicol via transforming to reusable magnetic composite. *Chem. Eng. J.* **322**, 571–581 (2017).
- Shang, J. G. *et al.* Removal of chromium (VI) from water using nanoscale zerovalent iron particles supported on herb-residue biochar. *J. Environ. Manag.* **197**, 331–337 (2017).
- Qian, L. B. *et al.* Nanoscale zero-valent iron supported by biochars produced at different temperatures: Synthesis mechanism and effect on Cr(VI) removal. *Environ. Pollut.* **223**, 153–160 (2017).
- Wang, S. S. *et al.* Biochar-supported nZVI (nZVI/BC) for contaminant removal from soil and water: A critical review. *J. Hazard. Mater.* **373**, 820–834 (2019).
- Zhang, D. J. *et al.* Enhanced nitrobenzene reduction by modified biochar supported sulfidated nano zerovalent iron: Comparison of surface modification methods. *Sci. Total Environ.* **694**, 133701 (2019).
- Chen, W., Pan, L., Chen, L., Wang, Q. & Yan, C. Dechlorination of hexachlorobenzene by nano zero-valent iron/activated carbon composite: Iron loading, kinetics and pathway. *RSC Adv.* **4**, 46689–46696 (2014).
- Maillard, M., Giorgio, S. & Pileni, M. P. Silver nanodisks. *Adv. Mater.* **14**, 1084–1086 (2002).
- Cao, G. H., Simon, P., Krämer, U., Wimbush, S. C. & Holzapfel, B. Transmission electron microscopy and high-resolution electron microscopy study of YNi₂B₂C thin film on Y₂O₃-Buffered MgO. *Chem. Mater.* **16**, 842–845 (2004).
- Wang, Y. N., Wei, J., She, Q., Pacheco, F. & Tang, C. Y. Microscopic characterization of FO/PRO membranes—a comparative study of CLSM, TEM and SEM. *Environ. Sci. Technol.* **46**, 9995–10003 (2012).
- Ren, C. L. *et al.* Synthesis of Ag/ZnO nanorods array with enhanced photocatalytic performance. *J. Hazard. Mater.* **182**, 123–129 (2010).

28. Lehman, J. H., Terrones, M., Mansfield, E., Hurst, K. E. & Meunier, V. Evaluating the characteristics of multiwall carbon nanotubes. *Carbon* **49**, 2581–2602 (2011).
29. Haigh, S. J. *et al.* Cross-sectional imaging of individual layers and buried interfaces of graphene-based heterostructures and superlattices. *Nat. Mater.* **11**, 764–767 (2012).
30. Bravman, J. C. & Sinclair, R. The preparation of cross-section specimens for transmission electron microscopy. *J. Electron. Microsc.* **1**, 53–61 (1984).
31. Liu, Y., Rafailovich, M. H., Sokolov, J., Schwarz, S. A. & Bahal, S. Effects of surface tension on the dislocation structures of diblock copolymers. *Macromolecules* **29**, 899–906 (1996).
32. Abrahams, M. S. & Buiocchi, C. Cross-sectional specimens for transmission electron-microscopy. *J. Appl. Phys.* **45**, 3315–3316 (1974).
33. Kim, D. H., Jang, Y., Park, Y. D. & Cho, K. Layered molecular ordering of self-organized poly(3-hexylthiophene) thin films on hydrophobized surfaces. *Macromolecules* **39**, 5843–5847 (2006).
34. Akamatsu, K. *et al.* Synthesis of pH-responsive nanocomposite microgels with size-controlled gold nanoparticles from ion-doped, lightly cross-linked poly(vinylpyridine). *Langmuir* **26**, 1254–1259 (2010).
35. Miyachi, M., Yamanoi, Y., Tomo, T. & Nishihara, H. Cross-sectional TEM analysis of an ITO surface coated with photosystem I and molecular wires. *J. Inorg. Organomet. P.* **26**, 1309–1312 (2016).
36. Moon, J. S., Lee, J. K., Cho, S., Byun, J. & Heeger, A. J. “Columnlike” structure of the cross-sectional morphology of bulk hetero-junction materials. *Nano Lett.* **9**, 230–234 (2009).
37. Oleksak, R. P. *et al.* Chemical and structural investigation of high-resolution patterning with HafSOx. *ACS Appl. Mater. Inter.* **6**, 2917–2921 (2014).
38. Yang, K., Jiang, Y., Yang, J. J. & Lin, D. H. Correlations and adsorption mechanisms of aromatic compounds on biochars produced from various biomass at 700 °C. *Environ. Pollut.* **233**, 64–70 (2018).
39. Yang, K., Zhu, L. H., Yang, J. J. & Lin, D. H. Adsorption and correlations of selected aromatic compounds on a KOH-activated carbon with large surface area. *Sci. Total. Environ.* **618**, 1677–1684 (2017).
40. Yang, K. *et al.* Are engineered nanomaterials superior adsorbents for removal and pre-concentration of heavy metal cations from water?. *Rsc Adv.* **4**, 46122–46125 (2014).
41. Yang, K. *et al.* Sorption of Cu²⁺ on humic acids sequentially extracted from a sediment. *Chemosphere* **138**, 657–663 (2015).
42. Wang, S. S. *et al.* The sorptive and reductive capacities of biochar supported nanoscaled zero-valent iron (nZVI) in relation to its crystallite size. *Chemosphere* **186**, 495–500 (2017).
43. Cao, Z., Li, H., Xu, X. & Xu, J. Correlating surface chemistry and hydrophobicity of sulfidized nanoscale zerovalent iron with its reactivity and selectivity for denitration and dechlorination. *Chem. Eng. J.* **394**, 124876 (2020).
44. Zhu, H. J., Jia, Y. F., Wu, X. & Wang, H. Removal of arsenic from water by supported nano zero-valent iron on activated carbon. *J. Hazard. Mater.* **172**, 1591–1596 (2009).
45. Lv, X., Xu, J., Jiang, G. & Xu, X. Removal of chromium(VI) from wastewater by nanoscale zero-valent iron particles supported on multiwalled carbon nanotubes. *Chemosphere* **85**, 1204–1209 (2011).
46. Devi, P. & Saroha, A. K. Synthesis of the magnetic biochar composites for use as an adsorbent for the removal of pentachlorophenol from the effluent. *Bioresour. Technol.* **169**, 525–531 (2014).
47. Brown, H. C. & Brown, C. A. A simple preparation of highly active platinum metal catalysts for catalytic hydrogenation. *J. Am. Chem. Soc.* **84**, 1494–1495 (1962).
48. Li, J., Fana, M. J., Li, M. & Liu, X. Cr(VI) removal from groundwater using double surfactant-modified nanoscale zero-valent iron (nZVI): Effects of materials in different status. *Sci. Total. Environ.* **717**, 137112 (2020).
49. Yang, K., Yang, J. J., Jiang, Y., Wu, W. H. & Lin, D. H. Correlations and adsorption mechanisms of aromatic compounds on a high heat temperature treated bamboo biochar. *Environ. Pollut.* **210**, 57–64 (2016).
50. Stefaniuk, M., Oleszczuk, P. & Ok, Y. S. Review on nano zerovalent iron (nZVI): From synthesis to environmental applications. *Chem. Eng. J.* **287**, 618–632 (2016).
51. Hussain, I. *et al.* Insights into the mechanism of persulfate activation with nZVI/BC nanocomposite for the degradation of non-ylphenol. *Chem. Eng. J.* **311**, 163–172 (2017).
52. Wu, J., Zheng, H., Zhang, F., Zeng, R. J. & Xing, B. S. Iron-carbon composite from carbonization of iron-crosslinked sodium alginate for Cr(VI) removal. *Chem. Eng. J.* **362**, 21–29 (2019).
53. Wylie, E. M., Olive, D. T. & Powell, B. A. Effects of titanium doping in titanomagnetite on neptunium sorption and speciation. *Environ. Sci. Technol.* **50**, 1853–1858 (2016).

Acknowledgements

This work was supported partly by the National Key Research and Development Program of China (2017YFA0207001, 2017YFC0211803), the National Natural Science Foundation of China (21777138, 21621005) and the Fundamental Research Funds for the Central Universities (2020FZZX001-06).

Author contributions

J.X.: writing-original draft. M.Z., D.L.: writing-review and editing. K.Y.: supervision, writing-review & editing.

Competing interests

The authors declare no competing interests.

Additional information

Supplementary Information The online version contains supplementary material available at <https://doi.org/10.1038/s41598-021-84685-w>.

Correspondence and requests for materials should be addressed to K.Y.

Reprints and permissions information is available at www.nature.com/reprints.

Publisher's note Springer Nature remains neutral with regard to jurisdictional claims in published maps and institutional affiliations.



Open Access This article is licensed under a Creative Commons Attribution 4.0 International License, which permits use, sharing, adaptation, distribution and reproduction in any medium or format, as long as you give appropriate credit to the original author(s) and the source, provide a link to the Creative Commons licence, and indicate if changes were made. The images or other third party material in this article are included in the article's Creative Commons licence, unless indicated otherwise in a credit line to the material. If material is not included in the article's Creative Commons licence and your intended use is not permitted by statutory regulation or exceeds the permitted use, you will need to obtain permission directly from the copyright holder. To view a copy of this licence, visit <http://creativecommons.org/licenses/by/4.0/>.

© The Author(s) 2021